Article

Angular Dependence of Strong Field Ionization of Haloacetylenes HCCX (X = F, Cl, Br, I), Using Time-Dependent Configuration Interaction with an Absorbing Potential

Paul Hoerner and H. Bernhard Schlegel*

Department of Chemistry, Wayne State University, Detroit, Michigan 48202, United States

ABSTRACT: Strong field ionization of haloacetylenes was simulated by time-dependent configuration interaction using all single excitations and a complex absorbing potential. The angular dependence of ionization for HCCX was mapped with static electric fields in the range 0.01−0.06 atomic units and compared with the results for CH_3X. HCCF ionizes primarily from the CC π orbital. HCCX (X = Cl, Br, I) compounds show increasing amounts of ionization from the halogen π-type lone pair orbitals and have a node perpendicular to the molecular axis. These shapes can be understood in terms of the energies and interactions of the halogen π-type lone pairs with the π orbitals of the CC triple bond.
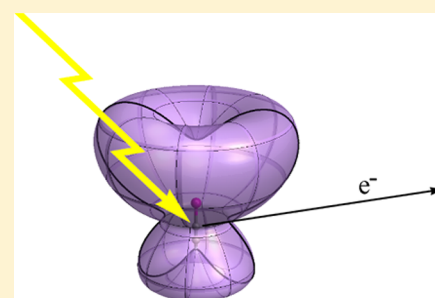
INTRODUCTION

The interaction between intense light and matter is dominated by electron dynamics. Recent advances in attosecond laser pulses have made it possible to study these dynamics on their natural time scale.[1−3] Early work in the field of attoscience showed that the ionization rate for CO and N_2 differed for molecules aligned with the field versus molecules perpendicular to the field.[4,5] Further studies have shown an angular dependence of ionization for CO_2, butadiene, and other polyatomic molecules.[6−10] The impact of the orientation of a molecule in the laser field on electron dynamics can also be deduced from high harmonic generation (HHG) spectra. Orbital tomography and HHG can be used to determine the shape of the highest occupied molecular orbital (HOMO).[11] Lower lying orbitals have also been found to contribute to HHG spectra at high intensities.[12−17]

For smaller molecules, the nodal structure of the molecular orbitals serves as a qualitative indicator of the angular dependence of ionization. For ionization in the tunneling regime, a better description can be obtained using molecular Ammosov−Delone−Krainov (ADK) theory.[18,19] Solving the time-dependent Schrödinger equation (TDSE) provides a more quantitative description of angular dependence of ionization and HHG spectra. The TDSE can be solved utilizing approximations such as single active electron, quantitative rescattering theory, time-dependent resolution in ionic states, time-dependent analytical R-matrix, and time dependent generalized active space configuration interaction.[20−24] In previous studies, we examined the angle dependence of various small molecules using a time-dependent configuration interaction (TDCI) approach with a complex absorbing potential (CAP).[25−31] In addition to a standard molecular basis, like aug-cc-pVTZ, the TDCI-CAP calculations need a large number of diffuse functions (which we termed the absorbing basis) to describe the electron density between the valence region and the complex absorbing potential (CAP).

A larger absorbing basis is needed for heavier elements, and this was developed using the methyl halides as a test case.[31]

Halogenated organic molecules have been the focus of several recent strong field studies.[32−56] Of particular interest for this study is the measurement of the electron dynamics of charge migration in iodoacetylene. It was found that the orientation of the molecule relative to the field made a significant contribution to the control over charge migration.[41] Dissociative single and double ionization of methyl iodide has recently been studied using 3D two-electron angular streaking (3D-2eAS) with double and quadruple coincidence detection of electrons and ions.[56] TDCI-CAP calculations were used to identify the relative contributions of the multiple orbitals involved in the single and double ionization of CH_3I and its subsequent fragmentation. A similar study of iodoacetylene is underway. In the present work, we use the TDCI-CAP method to examine the angular dependence of ionization and orbital contributions for the series of halogenated acetylenes HCCX (X= F, Cl, Br, or I) and compare the results to the corresponding series of methyl halides, CH_3X. These calculations provide the background needed for the analysis of the 3D-2eAS study of iodoacetylene.

METHODS

The electron dynamics in a strong field were simulated by solving the TDSE using the time-dependent configuration interaction approach with a complex absorbing potential, TDCI-CAP,

$$i\frac{\partial}{\partial t}\Psi_{el}(t) = [\hat{H}_{el} - \overset{\rightharpoonup}{\hat{\mu}} \cdot \vec{E}(t) - i\hat{\mathbf{V}}^{absorb}]\Psi_{el}(t) \tag{1}$$
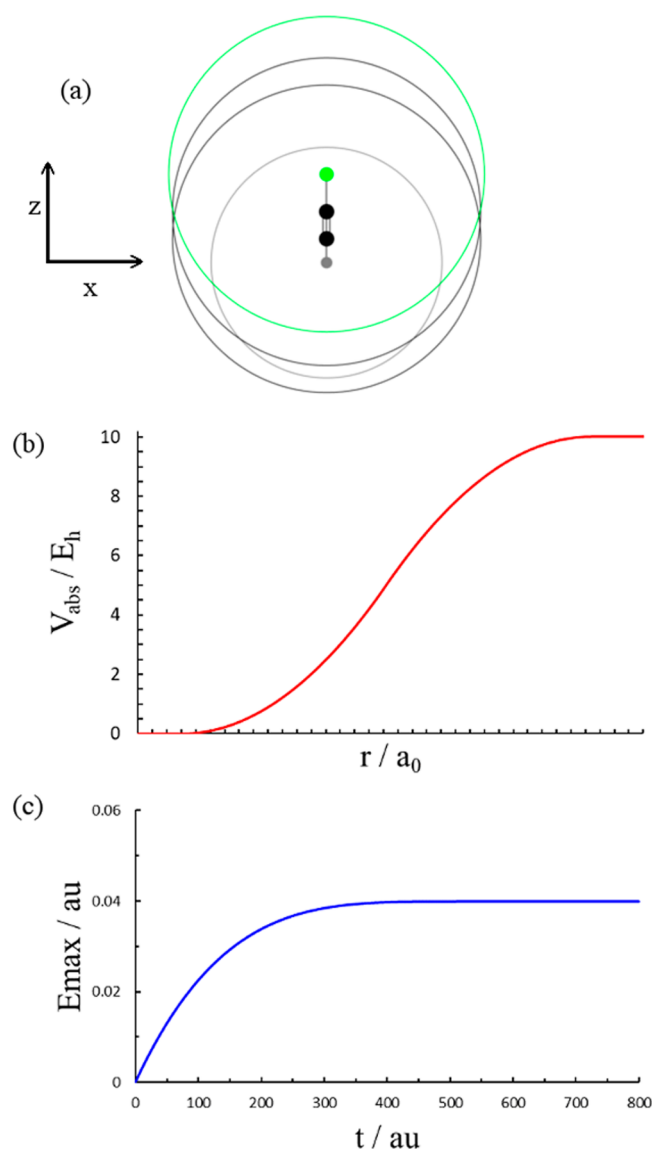
Figure 1. (a) Absorbing potential for the chloroacetylene molecule. (b) Radial part of the absorbing potential (the starting point is equal to the maxima of the starting radii for each atom). (c) Electric field used in the simulations (see eq 3).

$$\Psi_{el}(t) = \sum_{i=0} C_i(t)|\Psi_i\rangle \tag{2}$$

$\hat{H}_{el}$ is the field-free electronic Hamiltonian. The time-dependent wave function is expanded in terms of the Hartree–Fock ground state and all single excitations. The interactions between the field and wave function are modeled with the semiclassical dipole approximation with the dipole operator, $\vec{\mu}$, and the electric field, $\vec{E}$. As in our previous papers,[25–31] a complex absorbing potential (CAP), $-i\hat{V}^{absorb}$, was used to simulate ionization. The molecular CAP is constructed from spherical potentials centered on each atom, shown in Figure 1a. Each of the atomic potentials begins at 3.5 times the van der Waals radius of each element (R_H = 9.544 bohr, R_C = 12.735 bohr, R_F = 11.125 bohr, R_{Cl} = 13.052 bohr, R_{Br} = 13.853 bohr, R_I = 14.882 bohr) and rises quadratically to 5 hartree at approximately R + 14 bohr. The potential turns over quadratically to a constant value of 10 hartree at approximately R + 28 bohr (see Figure 1b). In order to use a

time-dependent approach to model ionization with a static field, the electric field is slowly ramped up to a constant value to avoid nonadiabatic excitations, as shown in Figure 1c. The electric field is given by

$$E(t) = E_{max}\left(1 - \left(1 - \frac{3}{2}\frac{t}{t_{max}}\right)^4\right) \quad \text{for } 0 \leq t \leq \frac{2}{3}t_{max};$$

$$E(t) = E_{max} \quad \text{for } t \geq \frac{2}{3}t_{max} \tag{3}$$

E_{max} is the maximum value for the electric field, and t_{max} = 800 au = 19.35 fs is the simulation time. To propagate the time-dependent wave function, a Trotter factorization of the exponential of the Hamiltonian is used:

$$\Psi(t + \Delta t) = \exp(-i\hat{H}\Delta t)\Psi(t)$$

$$\begin{aligned}\mathbf{C}(t + \Delta t) = {}&\exp(-i\mathbf{H}_{el}\Delta t/2)\exp(-\mathbf{V}^{absorb}\Delta t/2)\\ &\times \mathbf{W}^T \exp(iE(t + \Delta t/2)\mathbf{d}\Delta t)\mathbf{W}\\ &\times \exp(-\mathbf{V}^{absorb}\Delta t/2)\exp(-i\mathbf{H}_{el}\Delta t/2)\mathbf{C}(t)\end{aligned} \tag{4}$$

where $\mathbf{WDW}^T = \mathbf{d}$ are the eigenvalues and eigenvectors of the transition dipole matrix $\mathbf{D}$ in the field direction. $\mathbf{W}$, $\mathbf{d}$, $\exp(-i\mathbf{H}_{el}\Delta t/2)$ and $\exp(-\mathbf{V}^{absorb}\Delta t/2)$ are time independent and only need to be calculated once. A time step of Δt = 0.05 au (1.2 as) was used. Reducing the time step by half changed the norm at the end of the simulation by less than 0.01%.

A locally modified version of the Gaussian software package[57] was used to calculate all integrals needed for the TDCI-CAP simulation. In order to ensure sufficient interaction with the CAP, the standard Dunning aug-cc-pVTZ basis set[58–60] was augmented with additional diffuse basis functions (four s, four p, five d, and two f functions on each atom, absorbing basis C; see Table 1 of ref 31). The TDCIS wave function includes all single excitations from the occupied valence orbitals (e.g., 5s, 5p, and 4d orbitals on iodine) to all unoccupied orbitals with energies less than ~22 au, resulting in 1969, 2449, 3966, and 3979 configurations for HCCF, HCCCl, HCCBr, and HCCI, respectively. This absorbing basis has been previously tested for use with the halogen atoms.[31] An external Fortran90 code was used to carry out the TDCIS simulations and calculate the ionization rates. Figures 2–5 show the ionization rate, plotted as the radial distance from the center of the molecule in the direction that the electron is ejected. The resulting surface represents the angle-dependent ionization rate. The angles θ and ϕ were varied incrementally by 30° for a total of 62 directions for each E_{max}. For a smooth ionization surface plot, ionization yields were fitted to polynomials in $\cos(\theta)^n$, $\cos(m\varphi)$, and $\cos(\theta)^n \sin(m\varphi)$, n = 0–7, m = 0–6. Mulliken population analysis of the normalized one electron density of the absorbed wave function, $\hat{\mathbf{V}}^{absorb}\Psi_{el}(t)$, was used to determine the orbital contributions to ionization.

RESULTS AND DISCUSSION

The angular dependence of ionization for the haloacetylenes are shown in panel a of Figures 2–5. For HCCF, the result is essentially cylindrical with a node along the molecular axis in the +Z and −Z directions. By contrast, the plots for HCCX (X = Cl, Br, I) shows an additional node perpendicular to the molecular axis, resulting from the interaction of the halogen π-type lone pairs with the π orbitals of the CC triple bond. For HCCCl, the ionization rate is larger for the CC component; for HCCBr, the rates for the CC and bromine component are similar;
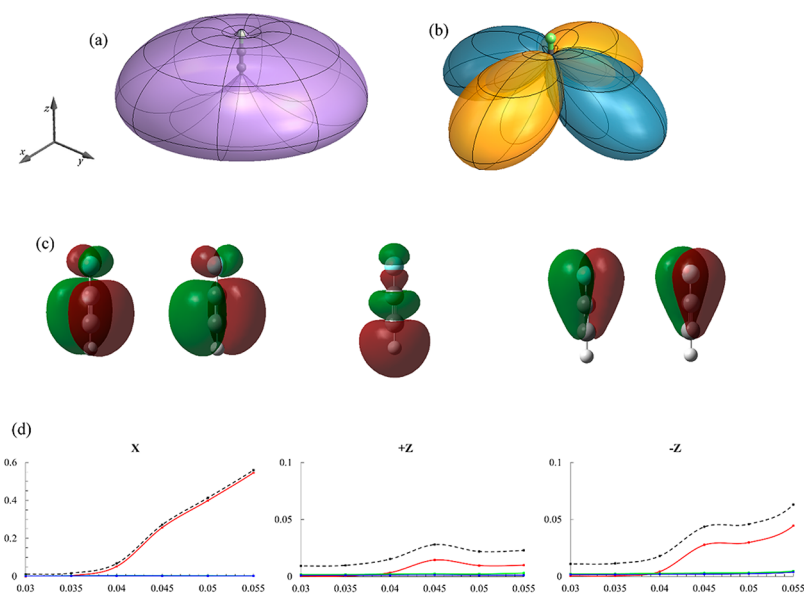
Figure 2. (a) Angular-dependent ionization yield of fluoroacetylene for a static pulse of maximum field strength 0.055 au. (b) Angular-dependent ionization contributions from the degenerate HOMO. (c) Highest occupied molecular orbitals (from left to right): degenerate π HOMO, σ HOMO−1, degenerate π HOMO−2. (d) Ionization rate (dashed) and contributions from degenerate π HOMO (red), σ HOMO−1 (green), and degenerate π HOMO−2 (blue) in the +X, +Z, and −Z directions as a function of field strength.
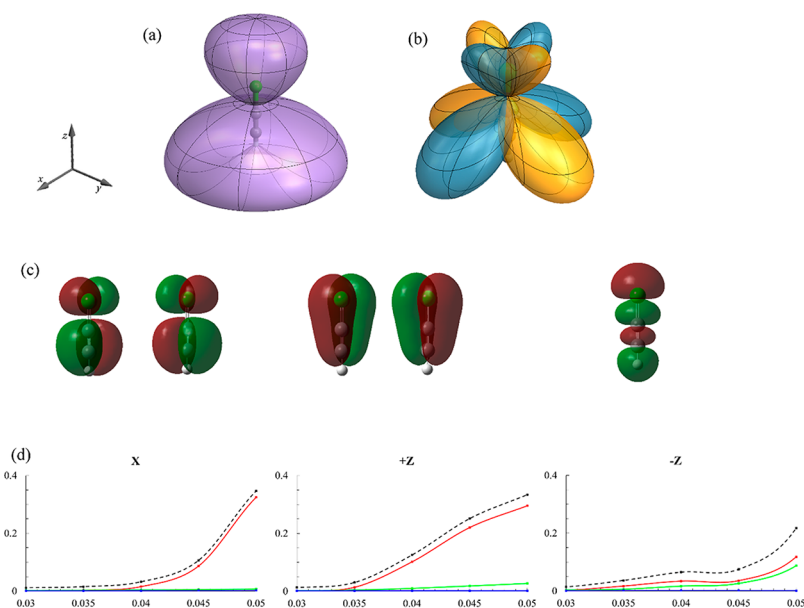

Figure 3. (a) Angular-dependent ionization yield of chloroacetylene for a static pulse of maximum field strength 0.050 au. (b) Angular-dependent ionization contributions from the degenerate HOMO. (c) Highest occupied molecular orbitals (from left to right): degenerate π HOMO, degenerate π HOMO−1, and σ HOMO−2. (d) Ionization rate (dashed) and contributions from degenerate π HOMO (red), degenerate π HOMO−1 (green), and σ HOMO−2 (blue) in the +X, +Z, and −Z directions as a function of field strength.

for HCCI, the iodine dominates. HCCCl and HCCBr also have significant ionization rates from the halogen end along the molecular axis. All of the haloacetylenes show a node in the ionization rate along the molecular axis at the hydrogen end of HCCX.

The trends in the shapes of the ionization rates for haloacetylenes are similar to the trends in the shapes for the halomethanes. CH_3F is dominated by ionization from the methyl group (Figure 3 of ref 31). For CH_3Cl and CH_3Br, there are increasing contributions from the halogen lone pair orbitals to the ionization rate (Figures 4 and 5 of ref 31). For CH_3I, ionization to the lowest energy cation is dominated by the iodine with very little contribution from the methyl group (Figure 6 of ref 31).

Mulliken population analysis can be used to obtain the orbital contributions to the angular dependence of the ionization rates. The contributions of the degenerate π HOMO to the ionization rate are illustrated in panel b of Figures 2−5; the molecular orbitals are shown in panel c of these figures. In HCCF, the HOMO has a small component from the fluorine, but this does not contribute significantly to the ionization rate. The component of the halogen π-type lone pairs in the HOMO of HCCX increases as X is incremented from Cl to Br to I. Because the HOMO is an out-of-phase combination of the CC π orbital and the halogen π-type lone pair orbitals, the HOMO has a node perpendicular to the molecular axis. As a result, the

Figure 4. (a) Angular-dependent ionization yield of bromoacetylene for a static pulse of maximum field strength 0.045 au. (b) Angular-dependent ionization contributions from the degenerate HOMO. (c) Highest occupied molecular orbitals (from left to right): degenerate π HOMO, degenerate π HOMO−1, and σ HOMO−2. (d) Ionization rate (dashed) and contributions from degenerate π HOMO (red), degenerate π HOMO−1 (green), and σ HOMO−2 (blue) in the +X, +Z, and −Z directions as a function of field strength.
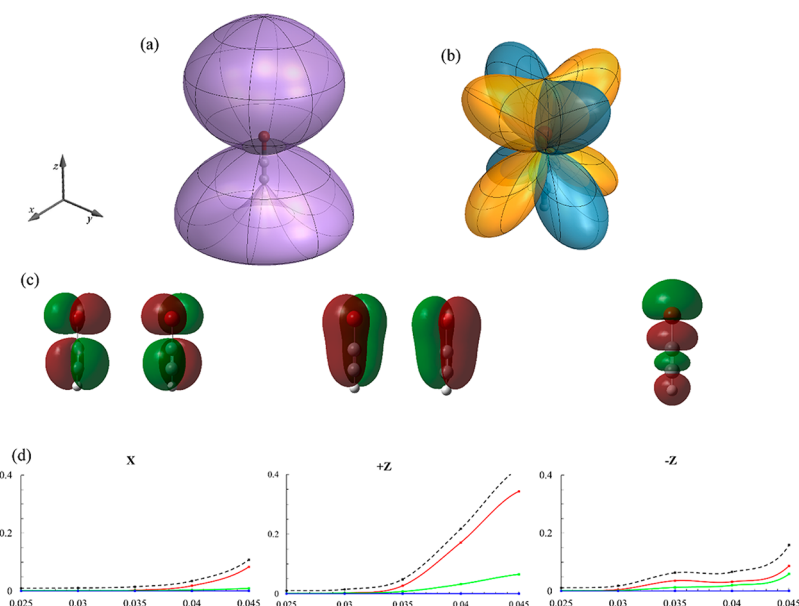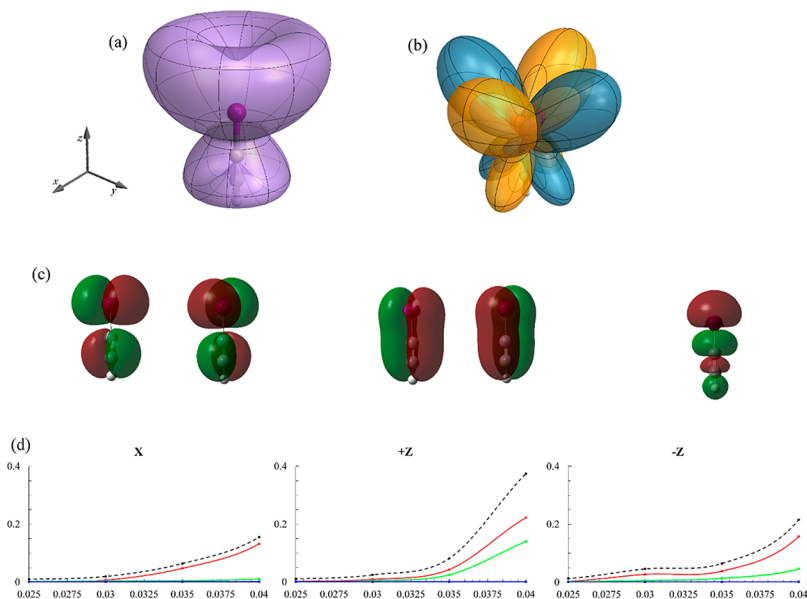

Figure 5. (a) Angular-dependent ionization yield of iodoacetylene for a static pulse of maximum field strength 0.040 au. (b) Angular-dependent ionization contributions from the degenerate HOMO. (c) Highest occupied molecular orbitals (from left to right): degenerate π HOMO, degenerate π HOMO−1, and σ HOMO−2. (d) Ionization rate (dashed) and contributions from degenerate π HOMO (red), degenerate π HOMO−1 (green), and σ HOMO−2 (blue) in the +X, +Z, and −Z directions as a function of field strength.

ionization rate also has a node perpendicular to the molecular axis. The contributions from HOMO−1 and HOMO−2 are much smaller than the contribution from HOMO.

The ionization yields as a function of the electric field are shown in panel d of Figures 2−5, along with the orbital components. Perpendicular to the molecular axis (X direction), the ionization yields are dominated by the HOMO, with almost no contributions from HOMO−1 or HOMO−2. Along the molecular axis, the ionization rate is higher from the halogen end of the molecule (+Z direction) than from the hydrogen end (−Z direction). In the +Z direction, the contributions of HOMO to the ionization dominate, but the contributions from

HOMO−1 increase from X = Cl to Br to I. For a given field strength, the trend in the ionization rate is F < Cl < Br < I, as expected from the energies of the HOMO.

The analysis of angular dependence of the ionization rate for HCCX and CH$_3$X shows that it is governed by the shapes and energies of the highest occupied orbitals with some contributions from HOMO−1. The energies of the π-type orbitals of HCCX and CH$_3$X are shown in Figure 6, along with the energies for the π-type lone pairs of atomic X (ROHF calculation with the same basis set) and the π HOMOs of HCCH and CH$_4$. Orbital π_1 (HOMO) is formed from an out-of-phase combination of the π-type lone pair orbitals of the halogen and
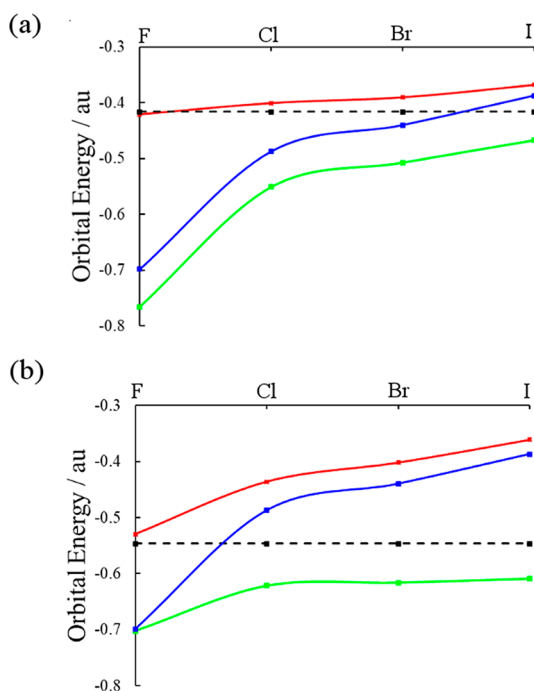
(a)

(b)

Figure 6. Orbital energies (in hartree) of (a) the π_1 and π_2 orbitals of HCCX (red and green), π-type lone pairs of X (blue), and the π orbitals of HCCH (dashed black) and (b) the π_1 and π_2 orbitals of CH$_3$X (red and green), π-type lone pairs of X (blue), and the π orbitals of CH$_4$ (dashed black).

the π orbital of HCCH or CH$_4$. Orbital π_2 is the in-phase combination of the π-type lone pair orbitals of the halogen and the π orbital of HCCH or CH$_4$ (HOMO−1 for HCCX (X = Cl, Br, I) or HOMO−2 for HCCF and CH$_3$X).

For HCCF, the π_1 energy is nearly equal to the energy of the π orbital for HCCH. Similarly, the π_1 energy for CH$_3$F is nearly equal to π for CH$_4$. The energy of π_2 is much lower and is nearly equal to the energy of the F lone pairs. Consequently, there is little mixing between the F π-type lone pairs and the π orbitals of HCCH or CH$_4$. Because the ionization rate is dominated by the higher lying π_1 orbital (HOMO), the ionization of HCCF is mainly from the π orbitals of the CC bond, and the ionization of CH$_3$F is mainly from the methyl group. This provides an explanation of the angular dependence of the ionization of HCCF and CH$_3$F.

For HCCX (X = Cl, Br, I), the energies of the halogen lone pairs are closer to but still lower than the energy of the HCCH π orbitals. Consequently, HOMO retains CC triple bond character. As X is incremented from Cl to Br to I, the halogen lone pair energies increase and the mixing with the HCCH π orbital increases, pushing the energy of π_1 slightly higher. Consequently, the ionization rate and the contribution from the halogen gradually increase. For CH$_3$X (X = Cl, Br, I), the energies of the halogen lone pairs are above the energy of the CH$_3$ π orbitals. Thus, the HOMO has mainly halogen character. As a result, ionization of CH$_3$I is mainly from the iodine lone pairs, whereas ionization of HCCI still has a significant amount of ionization from the π orbitals of the CC triple bond.

■ SUMMARY

The angular dependence of strong field ionization for haloacetylenes was examined for static fields in the range of 0.01−0.06 atomic units. Simulations were carried out using time-dependent configuration interaction with single excitations and a complex absorbing potential. The results were compared to the angular dependence of strong field ionization of CH$_3$X using the same approach. HCCF ionized almost exclusively from the CC fragment; similarly, CH$_3$F ionized mainly from the CH$_3$ fragment. HCCX and CH$_3$X (X = Cl, Br, I) showed increasing amounts of ionization from the halogen π-type lone pairs and a node perpendicular to the molecular axis. Ionization was found to occur primarily from the highest occupied molecular orbital, with smaller contributions from lower lying orbitals. The highest occupied orbitals are formed from halogen π-type lone pairs interacting with the π orbitals of the CC triple bond for HCCX and with the π orbitals of CH$_3$ for CH$_3$X. Because the π-type lone pair orbitals of fluorine are so much lower in energy than the π-type orbitals of CC or CH$_3$, fluorine does not contribute significantly to the highest occupied orbital or to the angular shape of the ionization. For X = Cl, Br, and I, the halogen lone pair orbitals are close enough in energy to the CC and CH$_3$ π orbitals to interact strongly. The out-of-phase interaction in the highest occupied orbital results in a node perpendicular to the molecular axis in the ionization yield. As the halogen is incremented from Cl to Br to I, ionization from the halogen end of the molecule becomes greater. For HCCX, the halogen lone pair orbitals are lower in energy than the CC π orbitals, and the shape of the ionization yield retains some CC character. For CH$_3$X, the halogen lone pair orbitals are higher in energy than the CH$_3$ π orbitals, and the shape of the ionization yield is dominated by the halogen lone pairs, especially for iodine.

■ AUTHOR INFORMATION

Corresponding Author

*E-mail: hbs@chem.wayne.edu. Phone: 313-577- 2562.

ORCID Ⓘ

H. Bernhard Schlegel: 0000-0001-7114-2821

Notes

The authors declare no competing financial interest.

■ REFERENCES

(1) Kling, M. F.; Vrakking, M. J. Attosecond Electron Dynamics. *Annu. Rev. Phys. Chem.* **2008**, *59*, 463−92.

(2) Gallmann, L.; Cirelli, C.; Keller, U. Attosecond Science: Recent Highlights and Future Trends. *Annu. Rev. Phys. Chem.* **2012**, *63*, 447−69.

(3) Krausz, F.; Ivanov, M. Attosecond Physics. *Rev. Mod. Phys.* **2009**, *81*, 163−234.

(4) Litvinyuk, I. V.; Lee, K. F.; Dooley, P. W.; Rayner, D. M.; Villeneuve, D. M.; Corkum, P. B. Alignment-Dependent Strong Field Ionization of Molecules. *Phys. Rev. Lett.* **2003**, *90*, 233003.

(5) Pinkham, D.; Jones, R. R. Intense Laser Ionization of Transiently Aligned CO. *Phys. Rev. A: At., Mol., Opt. Phys.* **2005**, *72*, 023418.

(6) Boguslavskiy, A. E.; Mikosch, J.; Gijsbertsen, A.; Spanner, M.; Patchkovskii, S.; Gador, N.; Vrakking, M. J. J.; Stolow, A. The Multielectron Ionization Dynamics Underlying Attosecond Strong-Field Spectroscopies. *Science* **2012**, *335*, 1336−1340.

(7) Mikosch, J.; Boguslavskiy, A. E.; Wilkinson, I.; Spanner, M.; Patchkovskii, S.; Stolow, A. Channel- and Angle-Resolved Above Threshold Ionization in the Molecular Frame. *Phys. Rev. Lett.* **2013**, *110*, 023004.

(8) Njoya, O.; Matsika, S.; Weinacht, T. Angle-Resolved Strong-Field Ionization of Polyatomic Molecules: More than the Orbitals Matters. *ChemPhysChem* **2013**, *14*, 1451−5.

(9) Pavicic, D.; Lee, K. F.; Rayner, D. M.; Corkum, P. B.; Villeneuve, D. M. Direct Measurement of the Angular Dependence of Ionization for N_2, O_2, and CO_2 in Intense Laser Fields. *Phys. Rev. Lett.* **2007**, *98*, 243001.

(10) Thomann, I.; Lock, R.; Sharma, V.; Gagnon, E.; Pratt, S. T.; Kapteyn, H. C.; Murnane, M. M.; Li, W. Direct Measurement of the Angular Dependence of the Single-Photon Ionization of Aligned N_2 and CO_2. *J. Phys. Chem. A* **2008**, *112*, 9382−6.

(11) Itatani, J.; Levesque, J.; Zeidler, D.; Niikura, H.; Pepin, H.; Kieffer, J. C.; Corkum, P. B.; Villeneuve, D. M. Tomographic Imaging of Molecular Orbitals. *Nature* **2004**, *432*, 867−871.

(12) Jin, C.; Bertrand, J. B.; Lucchese, R. R.; Worner, H. J.; Corkum, P. B.; Villeneuve, D. M.; Le, A. T.; Lin, C. D. Intensity Dependence of Multiple Orbital Contributions and Shape Resonance in High-Order Harmonic Generation of Aligned N_2 Molecules. *Phys. Rev. A: At., Mol., Opt. Phys.* **2012**, *85*, 013405.

(13) Le, A. T.; Lucchese, R. R.; Lin, C. D. Uncovering Multiple Orbitals Influence in High Harmonic Generation from Aligned N_2. *J. Phys. B: At., Mol. Opt. Phys.* **2009**, *42*, 211001.

(14) Li, J. W.; Liu, P.; Yang, H.; Song, L. W.; Zhao, S. T.; Lu, H.; Li, R. X.; Xu, Z. Z. High Harmonic Spectra Contributed by HOMO-1 Orbital of Aligned CO_2 Molecules. *Opt. Opt. Express* **2013**, *21*, 7599−7607.

(15) McFarland, B. K.; Farrell, J. P.; Bucksbaum, P. H.; Guhr, M. High Harmonic Generation from Multiple Orbitals in N_2. *Science* **2008**, *322*, 1232−1235.

(16) Smirnova, O.; Mairesse, Y.; Patchkovskii, S.; Dudovich, N.; Villeneuve, D.; Corkum, P.; Ivanov, M. Y. High Harmonic Interferometry of Multi-Electron Dynamics in Molecules. *Nature* **2009**, *460*, 972−977.

(17) Zhang, J. T.; Wu, Y.; Zeng, Z. N.; Xu, Z. Z. Intensity-Dependent Multiorbital Effect in High-Order Harmonics Generated from Aligned O_2 Molecules. *Phys. Rev. A: At., Mol., Opt. Phys.* **2013**, *88*, 033826.

(18) Ammosov, M. V.; Delone, N. B.; Krainov, V. P. Tunnel Ionization of Complex Atoms and of Atomic Ions in an Alternating Electromagnetic Field. *Sov. Phys. JETP* **1986**, *64*, 1191−1194.

(19) Tong, X. M.; Zhao, Z. X.; Lin, C. D. Theory of Molecular Tunneling Ionization. *Phys. Rev. A: At., Mol., Opt. Phys.* **2002**, *66*, 033402.

(20) Petretti, S.; Vanne, Y. V.; Saenz, A.; Castro, A.; Decleva, P. Alignment-Dependent Ionization of N_2, O_2, and CO_2 in Intense Laser Fields. *Phys. Rev. Lett.* **2010**, *104*, 223001.

(21) Le, A.-T.; Lucchese, R. R.; Tonzani, S.; Morishita, T.; Lin, C. D. Quantitative Rescattering Theory for High-Order Harmonic Generation from Molecules. *Phys. Rev. A: At., Mol., Opt. Phys.* **2009**, *80*, 013401.

(22) Spanner, M.; Patchkovskii, S. One-Electron Ionization of Multielectron Systems in Strong Nonresonant Laser Fields. *Phys. Rev. A: At., Mol., Opt. Phys.* **2009**, *80*, 063411.

(23) Torlina, L.; Ivanov, M.; Walters, Z. B.; Smirnova, O. Time-Dependent Analytical R-Matrix Approach for Strong-Field Dynamics. II. Many-Electron Systems. *Phys. Rev. A: At., Mol., Opt. Phys.* **2012**, *86*, 043409.

(24) Bauch, S.; Sørensen, L. K.; Madsen, L. B. Time-Dependent Generalized-Active-Space Configuration-Interaction Approach to Photoionization Dynamics of Atoms and Molecules. *Phys. Rev. A: At., Mol., Opt. Phys.* **2014**, *90*, 062508.

(25) Krause, P.; Sonk, J. A.; Schlegel, H. B. Strong Field Ionization Rates Simulated with Time-Dependent Configuration Interaction and an Absorbing Potential. *J. Chem. Phys.* **2014**, *140*, 174113.

(26) Krause, P.; Schlegel, H. B. Strong-Field Ionization Rates of Linear Polyenes Simulated with Time-Dependent Configuration Interaction with an Absorbing Potential. *J. Chem. Phys.* **2014**, *141*, 174104.

(27) Krause, P.; Schlegel, H. B. Angle-Dependent Ionization of Small Molecules by Time-Dependent Configuration Interaction and an Absorbing Potential. *J. Phys. Chem. Lett.* **2015**, *6*, 2140−6.

(28) Krause, P.; Schlegel, H. B. Angle-Dependent Ionization of Hydrides AH_n Calculated by Time-Dependent Configuration Interaction with an Absorbing Potential. *J. Phys. Chem. A* **2015**, *119*, 10212−20.

(29) Liao, Q.; Li, W.; Schlegel, H. B. Angle-Dependent Strong-Field Ionization of Triple Bonded Systems Calculated by Time-Dependent Configuration Interaction with an Absorbing Potential. *Can. J. Chem.* **2016**, *94*, 989−997.

(30) Hoerner, P.; Schlegel, H. B. Angular Dependence of Ionization by Circularly Polarized Light Calculated with Time-Dependent Configuration Interaction with an Absorbing Potential. *J. Phys. Chem. A* **2017**, *121*, 1336−1343.

(31) Hoerner, P.; Schlegel, H. B. Angular Dependence of Strong Field Ionization of CH_3X (X = F, Cl, Br, or I) Using Time-Dependent Configuration Interaction with an Absorbing Potential. *J. Phys. Chem. A* **2017**, *121*, 5940−5946.

(32) Corrales, M. E.; Gitzinger, G.; Gonzalez-Vazquez, J.; Loriot, V.; de Nalda, R.; Banares, L. Velocity Map Imaging and Theoretical Study of the Coulomb Explosion of CH_3I Under Intense Femtosecond IR Pulses. *J. Phys. Chem. A* **2012**, *116*, 2669−2677.

(33) De Nalda, R.; Rubio-Lago, L.; Loriot, V.; Banares, L. Femtosecond Photodissociation Dynamics by Velocity Map Imaging. The Methyl Iodide Case. *Springer Ser. Chem. Phys.* **2014**, *107*, 61−97.

(34) Ford, J. V.; Zhong, Q.; Poth, L.; Castleman, A. W. Femtosecond Laser Interactions with Methyl Iodide Clusters. I. Coulomb Explosion at 795 nm. *J. Chem. Phys.* **1999**, *110*, 6257−6267.

(35) Ford, J. V.; Poth, L.; Zhong, Q.; Castleman, A. W. Femtosecond Laser Interactions with Methyl Iodide Clusters. 2. Coulomb Explosion at 397 nm. *Int. J. Mass Spectrom.* **1999**, *192*, 327−345.

(36) Gitzinger, G.; Loriot, V.; Banares, L.; de Nalda, R. Pulse Shaping Control of CH_3I Multiphoton Ionization at 540 nm. *J. Mod. Opt.* **2014**, *61*, 864−871.

(37) Graham, P.; Ledingham, K. W. D.; Singhai, R. P.; Hankin, S. M.; McCanny, T.; Fang, X.; Kosmidis, C.; Tzallas, P.; Taday, P. F.; Langley, A. J. On the Fragment Ion Angular Distributions Arising from the Tetrahedral Molecule CH_3I. *J. Phys. B: At., Mol. Opt. Phys.* **2001**, *34*, 4015−4026.

(38) He, L.; Pan, Y.; Yang, Y.; Luo, S.; Lu, C.; Zhao, H.; Li, D.; Song, L.; Stolte, S.; Ding, D.; et al. Ion Yields of Laser Aligned CH_3I and CH_3Br from Multiple Orbitals. *Chem. Phys. Lett.* **2016**, *665*, 141−146.

(39) Karras, G.; Kosmidis, C. Multielectron Dissociative Ionization of CH_3I Clusters Under Moderate Intensity ps Laser Irradiation. *Int. J. Mass Spectrom.* **2010**, *290*, 133−141.

(40) Karras, G.; Kosmidis, C. Angular Distribution Anisotropy of Fragments Ejected from Methyl Iodide Clusters: Dependence on fs Laser Intensity. *Chem. Phys. Lett.* **2010**, *499*, 31−35.

(41) Kraus, P. M.; Mignolet, B.; Baykusheva, D.; Rupenyan, A.; Horný, L.; Penka, E. F.; Grassi, G.; Tolstikhin, O. I.; Schneider, J.; Jensen, F.; et al. Measurement and Laser Control of Attosecond Charge Migration in Ionized Iodoacetylene. *Science* **2015**, *350*, 790−795.

(42) Lai, Y. H.; Xu, J.; Szafruga, U. B.; Talbert, B. K.; Gong, X.; Zhang, K.; Fuest, H.; Kling, M. F.; Blaga, C. I.; Agostini, P.; DiMauro, L. F.; et al. Experimental Investigation of Strong-Field-Ionization Theories for Laser Fields from Visible to Midinfrared Frequencies. *Phys. Rev. A: At., Mol., Opt. Phys.* **2017**, *96*, 063417.

(43) Liu, H. T.; Yang, Z.; Gao, Z.; Tang, Z. Ionization and Dissociation of CH_3I in Intense Laser Field. *J. Chem. Phys.* **2007**, *126*, 044316.

(44) Ma, P.; Wang, C.; Li, X.; Yu, X.; Tian, X.; Hu, W.; Yu, J.; Luo, S.; Ding, D. Ultrafast Proton Migration and Coulomb Explosion of Methyl Chloride in Intense Laser Fields. *J. Chem. Phys.* **2017**, *146*, 244305.

(45) Ma, R.; Wu, C. Y.; Xu, N.; Huang, J.; Yang, H.; Gong, Q. H. Geometric Alignment of CH_3I in an Intense Femtosecond Laser Field. *Chem. Phys. Lett.* **2005**, *415*, 58−63.

(46) Siozos, P.; Kaziannis, S.; Kosmidis, C. Multielectron Dissociative Ionization of CH$_3$I Under Strong Picosecond Laser Irradiation. *Int. J. Mass Spectrom.* **2003**, *225*, 249−259.

(47) Sissay, A.; Abanador, P.; Mauger, F.; Gaarde, M.; Schafer, K. J.; Lopata, K. Angle-Dependent Strong-Field Molecular Ionization Rates with Tuned Range-Separated Time-Dependent Density Functional Theory. *J. Chem. Phys.* **2016**, *145*, 094105.

(48) Song, Y. D.; Chen, Z.; Sun, C. K.; Hu, Z. Angular Distributions of CH$_3$I Fragment Ions Under the Irradiation of a Single Pulse and Trains of Ultrashort Laser Pulses. *Chin. Phys. B* **2013**, *22*, 013302.

(49) Sun, S. Z.; Yang, Y.; Zhang, J.; Wu, H.; Chen, Y. T.; Zhang, S. A.; Jia, T. Q.; Wang, Z. G.; Sun, Z. R. Ejection of Triatomic Molecular Ion H$_3^+$ from Methyl Chloride in an Intense Femtosecond Laser Field. *Chem. Phys. Lett.* **2013**, *581*, 16−20.

(50) Tanaka, M.; Murakami, M.; Yatsuhashi, T.; Nakashima, N. Atomiclike Ionization and Fragmentation of a Series of CH$_3$-X (X: H, F, Cl, Br, I, and CN) by an Intense Femtosecond Laser. *J. Chem. Phys.* **2007**, *127*, 104314.

(51) Tang, X. F.; Zhou, X. G.; Wu, M. M.; Liu, S. L.; Liu, F. Y.; Shan, X. B.; Sheng, L. S. Dissociative Photoionization of Methyl Chloride Studied with Threshold Photoelectron-Photoion Coincidence Velocity Imaging. *J. Chem. Phys.* **2012**, *136*, 034304.

(52) Walt, S. G.; Ram, N. B.; von Conta, A.; Tolstikhin, O. I.; Madsen, L. B.; Jensen, F.; Worner, H. J. Role of Multi-Electron Effects in the Asymmetry of Strong-Field Ionization and Fragmentation of Polar Molecules: The Methyl Halide Series. *J. Phys. Chem. A* **2015**, *119*, 11772−11782.

(53) Wang, Y. M.; Zhang, S.; Wei, Z. R.; Zhang, B. Velocity Map Imaging of Dissociative Ionization and Coulomb Explosion of CH$_3$I Induced by a Femtosecond Laser. *J. Phys. Chem. A* **2008**, *112*, 3846−3851.

(54) Yang, Z.; Liu, H. T.; Tang, Z. C.; Gao, Z. Ionization and Dissociation of Methyl Bromide in Intense Laser Field. *Chem. J. Chin. Univ.* **2010**, *31*, 367−373.

(55) Zhang, D.; Luo, S.; Xu, H.; Jin, M.; Liu, F.; Yan, B.; Wang, Z.; Liu, H.; Jiang, D.; Eppink, A.; et al. Dissociative Ionization and Coulomb Explosion of CH$_3$I in Intense Femto Second Laser Fields. *Eur. Phys. J. D* **2017**, *71*, 148.

(56) Winney, A. H.; Basnayake, G.; Debrah, D.; Lin, Y. F.; Lee, S. K.; Hoerner, P.; Schlegel, H. B.; Li, W., Disentangling Strong Field Multi-Electron Dynamics with Angular Streaking. *J. Phys. Chem. Lett.*, manuscript under revision.

(57) Frisch, M. J.; Trucks, G. W.; Schlegel, H. B.; Scuseria, G. E.; Robb, M. A.; Cheeseman, J. R.; Scalmani, G.; Barone, V.; Petersson, G. A.; Nakatsuji, H., et al. *Gaussian Development Version*, revision I.09; Gaussian Inc.: Wallingford, CT, 2010.

(58) Dunning, T. H. Gaussian-Basis Sets for Use in Correlated Molecular Calculations 1. The Atoms Boron Through Neon and Hydrogen. *J. Chem. Phys.* **1989**, *90*, 1007−1023.

(59) Woon, D. E.; Dunning, T. H., Jr. Gaussian Basis Sets for Use in Correlated Molecular Calculations. III. The Atoms Aluminum Through Argon. *J. Chem. Phys.* **1993**, *98*, 1358−1371.

(60) Peterson, K. A.; Shepler, B. C.; Figgen, D.; Stoll, H. On the Spectroscopic and Thermochemical Properties of ClO, BrO, IO, and their Anions. *J. Phys. Chem. A* **2006**, *110*, 13877−13883.